Available online at www.sciencedirect.com

jmr&t Journal of Materials Research and Technology

www.jmrt.com.br

Original Article

The effect of heat treatment on the mechanical and tribological properties of dual size SiC reinforced A357 matrix composites

Avinash Lakshmikanthan[a,b], *T. Ram Prabhu*[c], *Udayagiri Sai Babu*[d], *Praveennath G. Koppad*[e], *Manoj Gupta*[f], *Munishamaiah Krishna*[g], *Srikanth Bontha*[a,*]

[a] *Department of Mechanical Engineering, National Institute of Technology, Surathkal 575025, India*
[b] *Department of Mechanical Engineering, Nitte Meenakshi Institute of Technology, Bangalore 560064, India*
[c] *CEMILAC, Defence R&D Organization, Bangalore 560093, India*
[d] *Department of Materials Engineering, Indian Institute of Science, Bengaluru 560012, India*
[e] *Department of Mechanical Engineering, Dayananda Sagar College of Engineering, Bengaluru 560078, India*
[f] *Department of Mechanical Engineering, The National University of Singapore, 10 Kent Ridge Crescent, 119260 Singapore, Singapore*
[g] *Department of Mechanical Engineering, RV College of Engineering, Bengaluru 560059, India*

ARTICLE INFO

Article history:
Received 21 February 2020
Accepted 7 April 2020
Available online 4 May 2020

Keywords:
Dual particle size (DPS) composites
Stir casting
T6 heat treatment
Microstructure
Mechanical properties
Aging
Wear

ABSTRACT

In the present work, the effect of aging temperature and particle size ratio of SiC particles on the mechanical and tribological properties of A357 composites reinforced with dual particle size SiC were investigated. The composites were prepared by melt-stirring assisted permanent mold casting technique with different weight fractions (3% coarse +3% fine, 4% coarse +2% fine, and 2% coarse +4% fine) of large and small size SiC particles. These three prepared composites are referred as DPS1, DPS2 and DPS3 composites. The solutionizing temperature was maintained constant at 540 °C for 9 h while the aging was done at 160 °C, 180 °C and 200 °C (T6 treatment) for 6 h. Optical and scanning electron microscopy studies showed fairly uniform dispersion of dual size SiC particles in A357 matrix with good interfacial bonding. High-resolution transmission electron microscopy images showed formation of uniformly dispersed needle-like β″ phase and spherical shaped β-Mg_2Si precipitates under peak aging conditions. Compared to T6 treated A357 alloy, the T6 treated DPS A357 composites showed improved yield strength, tensile strength, hardness and wear resistance. Among the three composites, hardness and wear resistance of T6 treated DPS2 composite was found to be significantly higher when compared to the other two composites (DPS1 and DPS3). Ratio of large particles to small particles also seems to effect the mechanical and tribological properties. Presence of more small particles was found to be good for strength and ductility whereas more large particles were found to be good for hardness and wear resistance.

* *Corresponding author.*
E-mail: srikanth.bontha@nitk.edu.in (S. Bontha).
https://doi.org/10.1016/j.jmrt.2020.04.027

1. Introduction

Owing to their low density, high specific strength, and high wear resistance, aluminum-based metal matrix composites are the most promising materials for various automotive and aerospace applications [1–4]. In particular, Al-Si-Mg alloys such as A356 and A357 are used in many critical applications like pistons, engine blocks, brake calipers, impellers, pump, and valve components. The primary reasons for using these alloys for above applications are their high specific strength, excellent weldability, castability, and good corrosion resistance. However, the mechanical properties are highly influenced by microstructure, chemical composition, solidification conditions, and heat treatment. The presence of Si and Mg along with appropriate heat treatment results in the formation of Mg_2Si precipitates, which improve the strength significantly. The general precipitation sequence can be given as, GP-I Zones → GP-II zones/β″ (Mg_5Si_6, FCC structure) → β′ Intermediate precipitate → β (Mg_2Si, hexagonal structure) precipitates. The age hardening response of A357 alloy largely depends on factors like chemical composition, solutionizing, and aging temperatures, which in turn determine the mechanical properties [5–9].

Al-Si alloy-based metal matrix composites are fabricated using both liquid and powder metallurgy routes. The selection of appropriate processing technique is based on the type and weight fraction of reinforcement, its morphology and the end application of the processed composite [10–15]. Canakci et al. [10,11] used powder processing technique for fabrication of Al based MMC's. Here they used methanol as a process control agent. They evaluated the microstructure and mechanical properties of the developed Al-MMC's. Canakci et al. used a novel method for the fabrication of AA7075 powders from recycled chips using mechanical milling [12]. Canakci et al. also used stir casting technique to fabricate AA2024 composite reinforced with B_4C particles and studied the effect of particle size, volume fraction, and wear behavior of the developed MMC's. Further artificial neural network (ANN) technique was used to predict the mechanical behavior of developed MMC's [13–15].

Zulfia et al. [16] in their work used a combination of stir casting and hot isostatic pressing techniques for fabrication of A357/SiC composites. The composites with 15% SiC were initially fabricated using stir casting followed by hot isostatic pressing at 550 °C. Badizi et al. [17] used stir casting technique to fabricate A357 composite with 1.5% SiC. They used a resistance furnace equipped with an electromagnetic stirrer to process the composite. In another work, Datta et al. [18] studied the corrosion behavior of powder metallurgy processed Al-Si-Mg/SiC composite. Elemental powders of Al, Si and Mg along with 2% SiC were mechanically alloyed, cold pressed and then sintered to obtain composite. Overall, stir casting technique is used to produce Al-Si composites owing to it flexibility and low cost of processing.

Taking a cue from its good manufacturing and mechanical characteristics, several efforts have been made to reinforce Al-Si-Mg alloy with ceramic particulates. The most commonly used ceramic particles include, SiC, TiC, TiB_2, and Al_2O_3, out of which SiC is an outstanding choice due to its low density, high hardness, high elastic modulus and excellent chemical inertness. Yu et al. [19] studied the reinforcing mechanism of TiB_2 in as-cast A357/TiB_2 in situ composites. It was observed that mechanical properties increased due to an increase in dislocation density near the boundary of α-Al and TiB_2 particles. Kandemir et al. [20] studied the microstructure, and mechanical properties of SiC reinforced A357 composites processed by ultrasonic cavitation method. The hardness and tensile strength of the composite increased from 60 HV and 138 MPa to 73 HV and 198 MPa respectively when A357 alloy was reinforced with SiC particles. The strengthening in the composite was attributed to grain size reduction and Orowan mechanism. However, the effect of load-bearing mechanism was found to be minimal. Leonard et al. [21] compared the sliding wear behavior of A357 alloys and 30 vol% SiC reinforced A357 composites at different loads ranging from 6–74 N. They observed that at a lower load of 6 N, the average wear coefficient of the composite was found to be significantly lower than that of the alloy. At a higher load of 74 N, the average wear coefficient and depth of deformation of the composite was twice that of the alloy.

On the other hand, several works reported the effect of heat treatment on mechanical properties of A357 and its composites. Bloyce and Summers [22] studied the effect of heat treatment on mechanical properties of A357/SiC composites. Out of the two heat treatment procedures opted, the one with 540 °C solutionizing and 160 °C aging temperature showed better mechanical properties for both A357 alloy and composites. Taghiabadi et al. [23] reported the effect of heat treatment on as cast Al-Si-Mg composites reinforced with TiB_2 particles. Tensile strength of the heat-treated composites was found to be higher due to the strengthening effect provided by Mg_2Si precipitates. Strengthening in age hardened A356/TiB_2 composites was attributed to the formation of β′, β (Mg_2Si) precipitates. Dislocation pining, and their pileups in the vicinity of TiB_2particles were also reported [24]. It is well known that the mechanical properties like strength and wear resistance of composites largely depend on the size, amount, morphology and dispersion of reinforcement in the metal matrix. In particular, the effect of size of particles plays a vital role in deciding the strength and ductility of the resulting composites. Micron-sized particles improve strength at the cost of significant loss in ductility while sub-micron or nano-sized particles improve not only the strength but also the ductility. This has led to several studies on the development of bimodal or trimodal particle reinforced composites [24–27]. Bindumadhavan et al. [25] studied the effect of dual size SiC (47 and 120 μm) on impact energy and wear rate of Al-Si-Mg composites. The impact energy of dual size SiC composite (12.2 J) was much higher than that of single particle size composite (6.7 J). Further, the weight loss during wear test was less in case of dual size SiC composite (30 mg) while higher in case of single particle size composite (47 mg). Sharma et al. [28] studied the effect of bimodal sillimanite (1–20 μm and 75–106 μm) on dry sliding wear behavior of Al-Si composites fabricated by stir casting technique. Al-Si composite having a higher weight fraction of small-sized particles and lower weight fraction of large particles (3:1) showed the highest nano-hardness and lowest wear rate when compared to other combinations. Overall bimodal sized reinforcement-based composites are quite

attractive over conventional composites with single size reinforcement. So far, limited work has been reported on the effect of heat treatment on mechanical and tribological properties of A357 composite reinforced with bimodal SiC particles. The other aspect which is not yet studied systematically is the effect of ratio of large to small particles on the mechanical and tribological properties. Finding the optimum ratio of large to small particle size and variation of properties with this ratio is expected to provide more insights into the role of bimodal particle reinforcements in improving properties of composites.

In the present work, an attempt is made to understand the effect of heat treatment on the mechanical and tribological properties of A357 composites reinforced with dual size SiC particles. The effect of solutionizing and various aging temperatures along with different weight fractions of dual size SiC particles on microstructure, strength, and wear resistance is studied. The study will further the understanding of effect of aging temperature and ratio of large to small particle size on properties of A357 composites reinforced with dual size SiC particles.

2. Experimental procedures

2.1. *Materials and DPS-SiC composite fabrication method*

Al-7.4Si-0.54 Mg (A357 alloy) with a theoretical density of 2.7 g/cc was selected as a matrix material, and SiC of two different particle sizes (140 ± 10 μm (Large) and 30 ± 5 μm (Small)) having a density 3.21 g/cc [29] were used as reinforcements. The SiC powder samples (two different mesh sizes) and their morphology with EDS analysis are shown in Fig. 1(a)–(d). The fabrication of A357 dual particle size composites has been described in detail in our previous work [30,31]. Images of cast sample are shown in Fig. 2. The process flowchart for fabrication of A357 composite reinforced with dual size SiC particles is presented in Fig. 3.

As-cast A357 alloy and its DPS composites were subjected to T6 heat treatment or precipitation treatment using a muffle furnace equipped with a temperature controller. The T6-heat treatment process consists of solutionizing, quenching, and aging. The as-cast A357 alloy and its DPS composites were T6 heat treated using temperature-time cycles as shown in Fig. 4 and the description is provided below.

Step 1: Solutionizing at a temperature of 540 °C ± 2 °C for 9 h which is widely used for production of A357 alloys and its composites [32–34].
Step 2: Quenching in water to room temperature with a quench delay time restricted to 5–6 s.
Step 3: Aging in a temperature range of 160 °C to 200 °C in steps of 20 °C for 6 h.

The precipitation heat-treatment (T6) cycles shown in Fig. 4 for different cases are designated as follows:

(a) 540 °C (Solution Treatment) for 9 h – quenching in water –160 °C (aging) for 6 h is denoted by 540-9H-160-6H.
(b) 540 °C (Solution Treatment) for 9 h – quenching in water –180 °C (aging) for 6 h is denoted by 540-9H-180-6H.

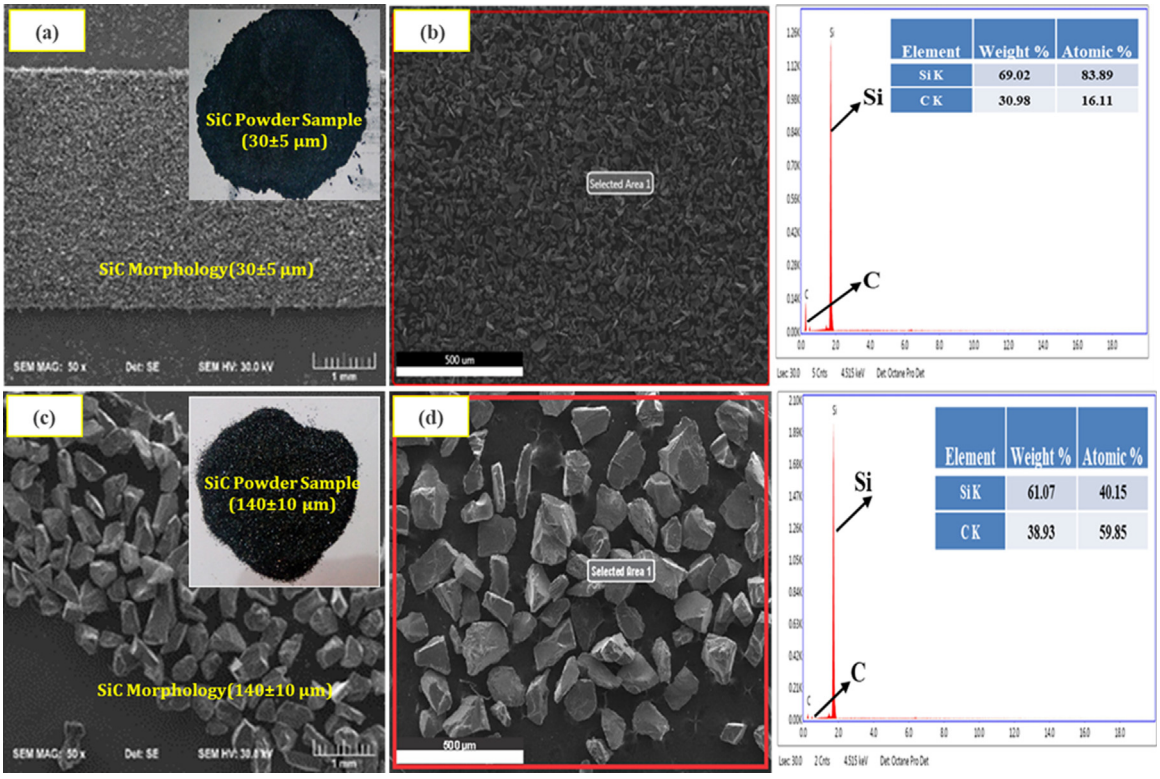

Fig. 1 – Morphology of SiC particles, (a) SiC powder sample (fine size) (b) Morphology of fine size SiC particles with EDS analysis (c) SiC powder sample (coarse size) and (d) Morphology of coarse size SiC particles with EDS analysis.

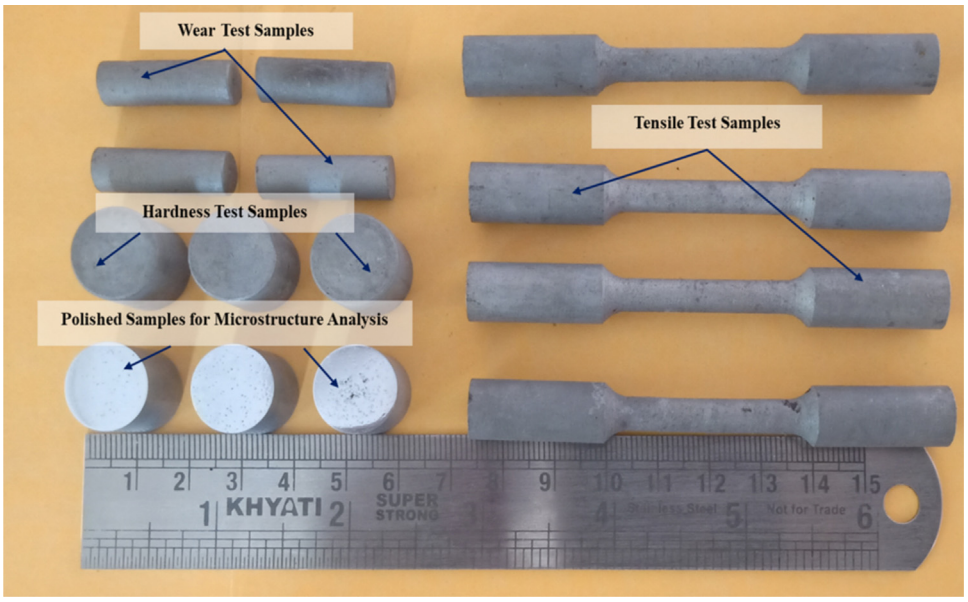

Fig. 2 – Images of cast samples.

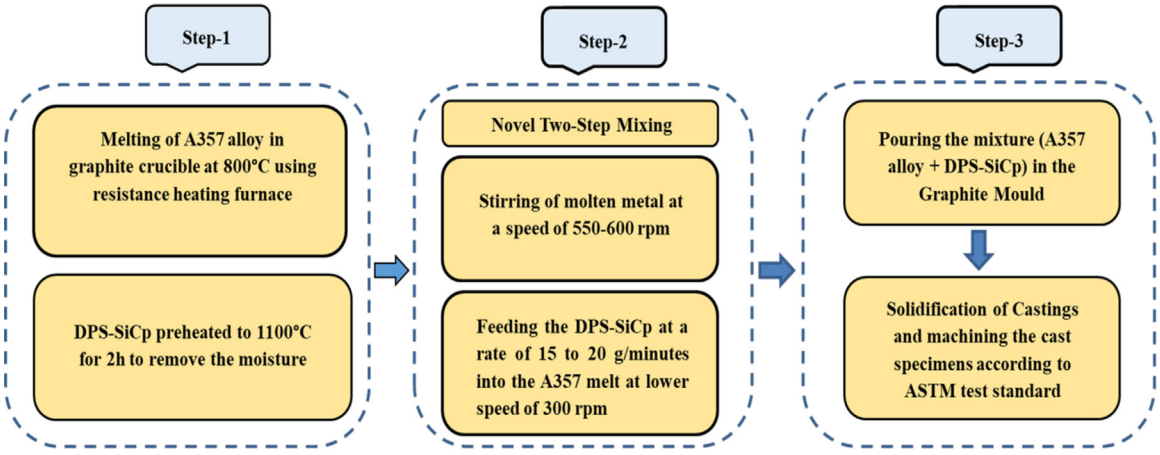

Fig. 3 – Process flowchart for fabrication of A357 composite reinforced with dual size SiC particles.

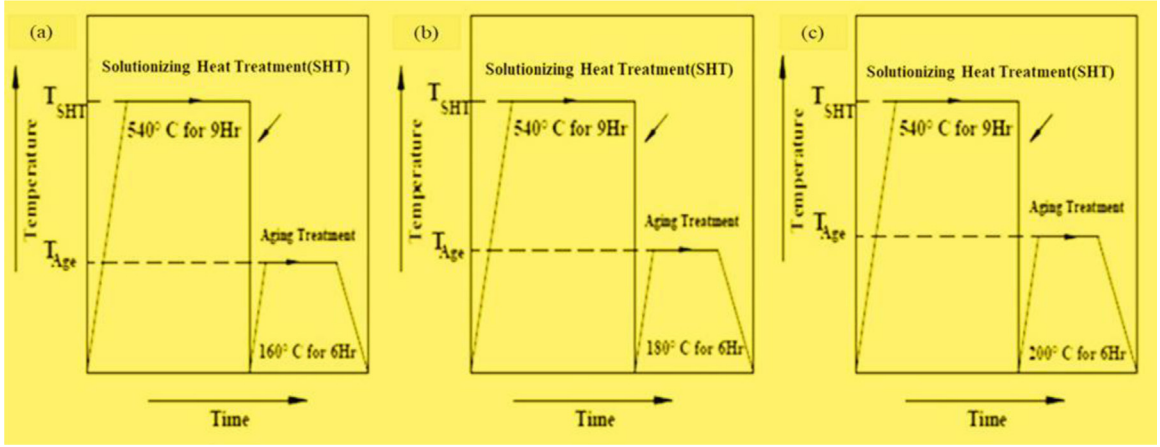

Fig. 4 – Precipitation heat treatment (T6) cycles.

Table 1 – The alloy/composite, heat treatment, weight fraction of SiC particles and their designation. Herein, L:S corresponds to ratio of wt. % of coarse (140 ± 10 μm-L) and fine (30 ± 5 μm-S) particles of Dual Particle Size SiC.

Alloy/Composite	Heat Treatment (T6- treated)	L:S (wt. %)	Designation
As-Cast A357 alloy	540-9H-160-6H	Nil	A357-160 °C – 6H
As-Cast A357 alloy	540-9H-180-6H		A357-180 °C – 6H
As-Cast A357 alloy	540-9H-200-6H		A357-200 °C – 6H
DPS 1 Composite	540-9H-160-6H	3:3	DPS1-160 °C – 6H
DPS 1 Composite	540-9H-180-6H		DPS1-180 °C – 6H
DPS 1 Composite	540-9H-200-6H		DPS1-200 °C – 6H
DPS 2 Composite	540-9H-160-6H	4:2	DPS2-160 °C – 6H
DPS 2 Composite	540-9H-180-6H		DPS2-180 °C – 6H
DPS 2 Composite	540-9H-200-6H		DPS2-200 °C – 6H
DPS 3 Composite	540-9H-160-6H	2:4	DPS3-160 °C – 6H
DPS 3 Composite	540-9H-180-6H		DPS3-180 °C – 6H
DPS 3 Composite	540-9H-200-6H		DPS3-200 °C – 6H

(c) 540 °C (Solution Treatment) for 9 h – quenching in water –200 °C (aging) for 6 h is denoted by 540-9H-200-6H.

The alloy/composite, heat treatment, weight fraction of SiC particles and their designation is presented in Table 1.

2.2. *Phase analysis and Microstructural characterization*

The heat-treated samples (A357 alloy and its DPS composites) were further characterized as per suitable ASTM standards. The characterization and testing carried out on these samples is summarized in Fig. 5.

XRD analysis of samples was conducted using X'Pert^3 Powder diffractometer (PANalytical, Malvern, UK) with CuKα radiation. The study was performed for the scan angle range of 20° to 80° at a scan speed of 2°/min. Before XRD studies, the samples were cleaned with acetone and were also dried in air. Using standard metallurgical procedures as per ASTM E3-17 standards the composites were polished and etched with Keller's reagent. Optical (Model: Nikon LV150) and scanning electron microscopy (Model: TESCAN Vega 3 LMU) studies were carried out to check the dispersion and bonding of SiC particles with A357 matrix. In order to study the precipitates and dislocations, transmission electron microscopy examination was conducted using JEOL JEM 2100 High Resolution Transmission Electron Microscope (HRTEM). For this, samples of 3 mm diameter and 10 μm thick were prepared using ion beam milling (Model 691, Gatan).

2.3. *Density measurements*

The experimental density (ρ_{exp}) of the A357 alloy and its DPS composites was measured using the Archimedes principle (ASTM D792-66 standard) and, the theoretical density (ρ_{th}) was calculated using the rule of mixtures [13,14,35,36].

2.4. *Mechanical and wear testing*

The hardness test was carried out using a Micro Cum Macro-Vickers hardness testing machine (Model: VH1150) as per ASTM E384 standard. Tensile test was conducted as per

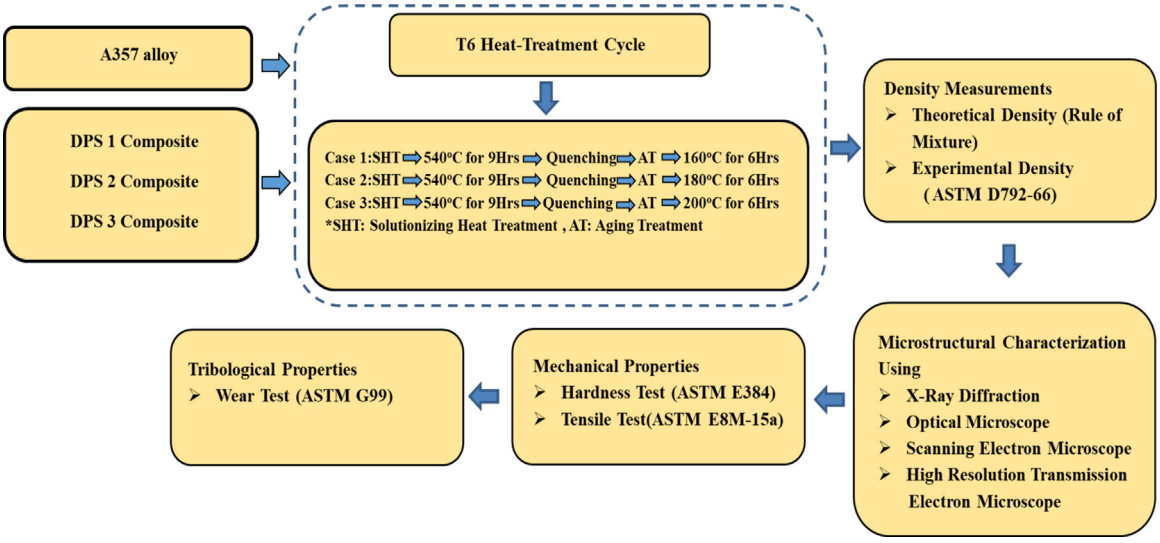

Fig. 5 – Flowchart of characterization and testing carried out on DPS-SiC reinforced A357 MMCs.

Table 2 – Theoretical density (ρ_{th}) and experimental density (ρ_{exp}) of A357 alloy and its DPS composites (T6-heat treated).

S/No	Alloy/Composite	Designation	Theoretical density (gm/cc)	Experimental density (gm/cc)
1	As-Cast A357 alloy	A357-160°C – 6H	2.700	2.685
2	DPS 1 Composite	DPS1-160°C – 6H	2.730	2.713
3	DPS 2 Composite	DPS2-160°C – 6H	2.730	2.715
4	DPS 3 Composite	DPS3-160°C – 6H	2.730	2.713
5	As-Cast A357 alloy	A357-180°C – 6H	2.700	2.691
6	DPS 1 Composite	DPS1-180°C – 6H	2.730	2.720
7	DPS 2 Composite	DPS2-180°C – 6H	2.730	2.721
8	DPS 3 Composite	DPS3-180°C – 6H	2.730	2.720
9	As-Cast A357 alloy	A357-200°C – 6H	2.700	2.688
10	DPS 1 Composite	DPS1-200°C – 6H	2.730	2.717
11	DPS 2 Composite	DPS2-200°C – 6H	2.730	2.718
12	DPS 3 Composite	DPS3-200°C – 6H	2.730	2.716

ASTM E8M-15a standard to evaluate the yield strength, tensile strength and ductility of the heat-treated composites. Tribological properties i.e. wear rate was obtained by conducting dry sliding wear test using pin-on-disc machine (Model TR-20LE, Ducom, India) as per ASTM-G99 standard. For wear tests, applied load was varied from 10 N to 30 N in steps of 5 N at a fixed sliding velocity of 2.5 m/sec and sliding distance of 1500 m. Fracture surfaces after tensile test, worn surface and wear debris after wear test were studied using scanning electron microscope.

3. Results and discussion

3.1. *Density measurement results of A357 alloy and its DPS composite at T6-heat treated condition*

Table 2 shows the density measurements (theoretical and experimental) of A357 alloy and its DPS composites at varying aging temperatures (160 °C, 180 °C, and 200 °C). The density values of the DPS composites are slightly higher compared to the A357 alloy. This is due to the presence of a high-density ceramic material (SiCp) [13,37]. Variations in the density among the composites heat treated to different conditions are negligible. From Table 2, we can observe that the difference in the theoretical and experimental densities is insignificant. Thus, it can be concluded that the dispersion of SiC particles was found to be good with almost no observable porosity or any casting defects [38,39].

3.2. *Phase analysis of A357 alloy at T6-heat treated condition*

Fig. 6 shows the XRD patterns of A357 alloy at different aging temperatures (160 °C, 180 °C, and 200 °C). The XRD analysis of A357 alloy reveals the presence of Al and Si as major peaks. In addition, small peaks of Mg and Mg_2Si intermetallic phases were detected which shows that Mg and Si form the Mg_2Si intermetallic precipitates as shown by EDS analysis. From the figure, it can be observed that as the aging temperature increases, the intensity of the peaks also increases. Similar trends have been reported in literature [40].

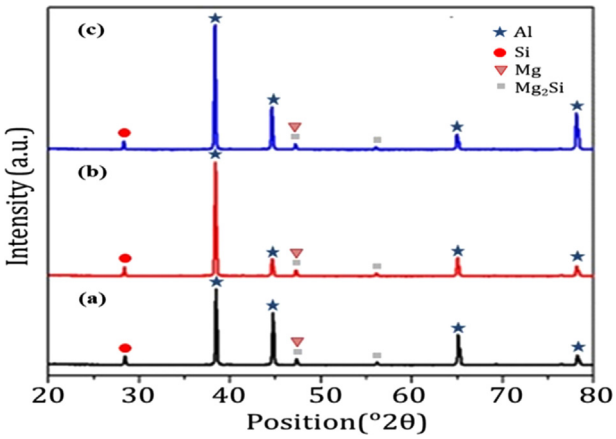

Fig. 6 – (a) XRD patterns of A357 alloy at different aging temperatures (a) XRD pattern of A357 alloy at 540 °C-9H-160 °C-6H (b) XRD pattern of A357 alloy at 540 °C-9H-180 °C-6H (c) XRD pattern of A357 alloy at 540 °C-9H-200 °C-6H.

3.3. *Microstructural analysis of A357 alloy at different conditions (un-treated and T6-heat treated)*

Fig. 7(a) shows the optical micrograph of as-cast A357 alloy (untreated condition). The micrograph consists of two phases namely α-Al phase and Al-Si eutectic phase. The microstructure is largely dominated by coarse size α-Al grains which are surrounded by eutectic Si regions repeated in periodic cell patterns that are fibrous in shape.

Fig. 7(b) and (c) show the optical micrographs of A357 alloy solution treated at 540 °C and aged at 180 °C and 200 °C respectively. In Fig. 7(b) fine globular morphology of eutectic silicon particles due to heat treatment can be observed. Similar results were reported by researchers [41,42]. Heat treatment results in the transformation of fibrous shape eutectic Si into fine spheroidized Si particles uniformly distributed in the A357 matrix. Heat treatment also dissolves Mg_2Si particles, results in structural homogenization, and alters the shape of eutectic Si particles. Upon heat treatment necking can be seen in Si particles. With further increase in temperature from 160–180 °C, particle fragmentation and spherodization

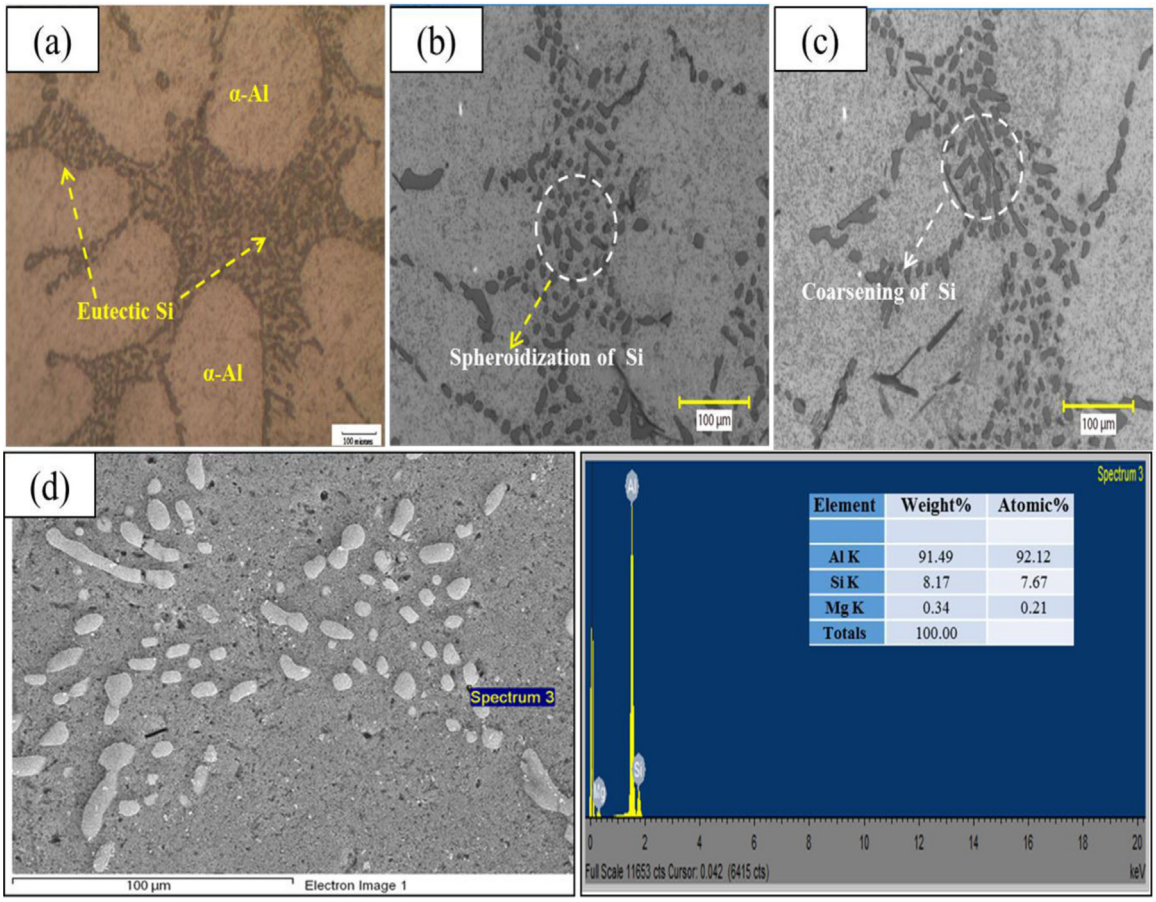

Fig. 7 – (a) Optical micrograph of as-cast A357 alloy (untreated condition) (b) Optical micrograph of as-cast 357 alloy at 540 °C-9H-180 °C-6H (c) Optical micrograph of as-cast 357 alloy at 540 °C-9H-200 °C-6H (d) SEM micrograph with EDS spectrum at 540 °C-9H-180 °C-6H.

takes place (Fig. 7(b)) [32,33]. Further, from Fig. 7(b) it can be observed that the Si particles are smaller and more uniformly distributed. The fragmentation of Si particles reduces the particle size and increases particle number, which in turn leads to the strengthening of the alloy. As the aging temperature is increased from 180 °C to 200 °C, coarsening of Si particles can be observed (Fig. 7(c)).

Fig. 7(d) shows the SEM micrograph with EDS spectrum of A357 alloy solution treated at 540 °C and aged at 180 °C. From the EDS spectrum, traces of Mg located at the Al-Si interfaces can be found. Typically, Mg is added to the Al–Si alloy for age hardening through the precipitation of Mg_2Si precipitates. In Fig. 7(d), magnesium peak from the EDS analysis confirms that Mg_2Si precipitates form as a result of heat treatment.

3.4. *Microstructural analysis of DPS composite at T6-heat treated condition*

Fig. 8(a)–(c) shows the optical micrographs of heat-treated composites (solution treated at 540 °C and aged at 180 °C) DPS1, DPS2 and DPS3 respectively. It can be observed from all the micrographs that both dual sizes SiC particles were found to be fairly uniformly distributed in the A357 matrix. Fig. 8(a) shows micrograph of DPS1 composite where the dispersion of SiC particles was found to be very good with almost no observable porosity or any casting defects. However, a small extent of clustering of small size SiC particles was observed in the case of DPS2 composite as shown in Fig. 8(b). Most of the SiC particles seen in microstructure are of large size, which is due to the high content of large size particles when compared to small size particles. On the other hand, the dispersion of particles in DPS3 composite was reasonably uniform, as shown in Fig. 8(c). Small-scale cluster formation of small size SiC particles were seen at few spots closer to large SiC particles in DPS3 composite. High shear rate generated during melt-stirring process pushes small size particles at a faster rate when compared to large particles. However, the movement of small particles is restricted by large particles due to which they get settled near them, and same is seen in Fig. 8(b). Overall dispersion of dual size SiC particles was found to be reasonably uniform in all the composite systems, and hardly any casting defect like porosity was seen on the surface. The addition of SiC as reinforcement enhances aging kinetics, phase formation reaction and it also acts as seeding for precipitation during the heat treatment process, which further leads to alloy strengthening [43–45]. These dual sizes SiC particles influence the strengthening of matrix material in a significant way during the heat treatment process [45–48].

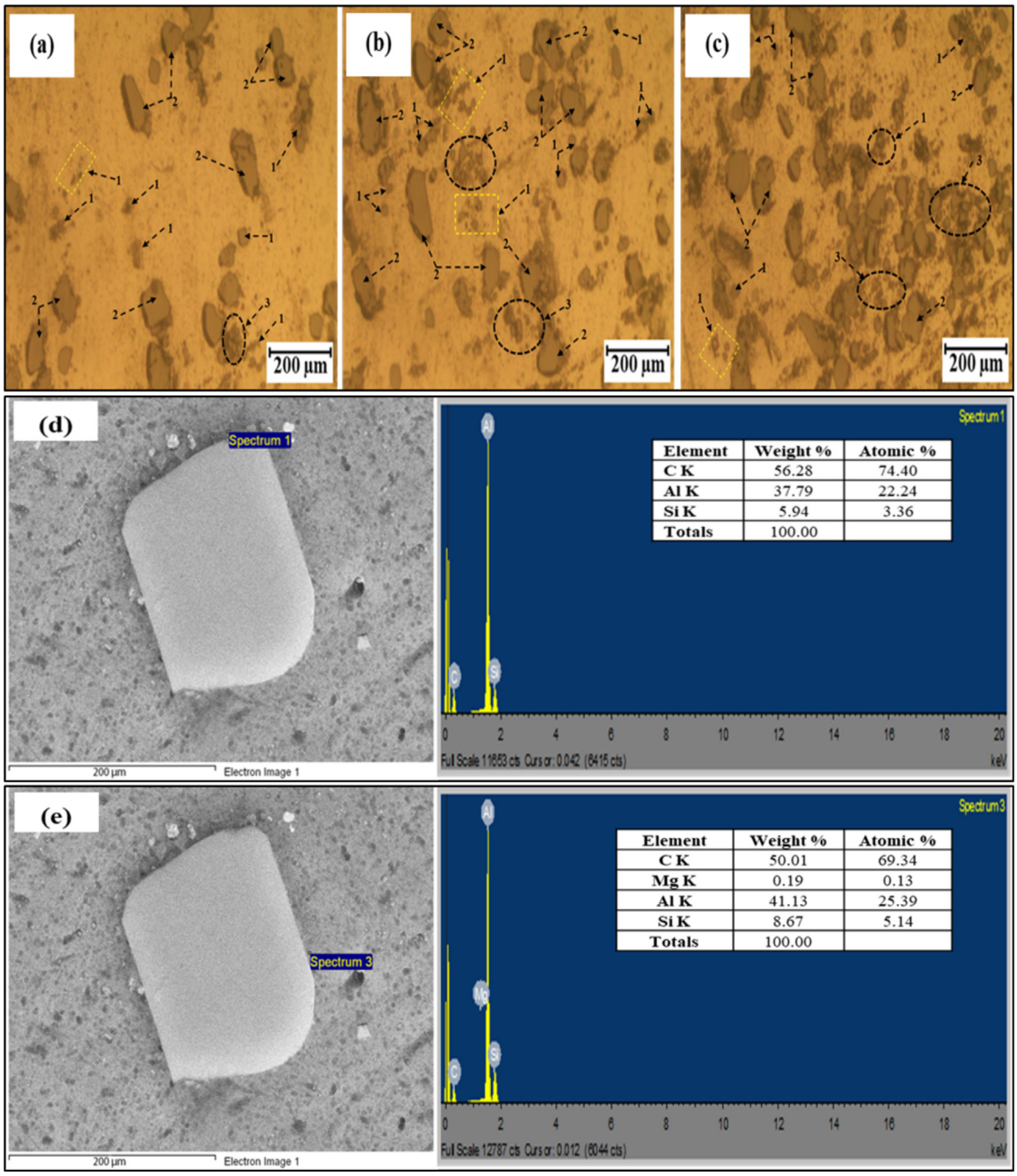

Fig. 8 – Micrographs of DPS composites aged at 540 °C-6H-180 °C conditions. (a) Optical micrograph of DPS1 composite at 180 °C (b) Optical micrograph of DPS2 composite at 180 °C (c) Optical micrograph of DPS3 composite at 180 °C. In (a)–(c), 1 represents fine SiCp,2 represents coarse SiCp, 3 shows clustering of fine SiCp (d) EDS spectrum taken on DPS2 composite particle and (e) EDS spectrum at Al/SiC interface.

Fig. 8(d) shows the EDS analysis of composite particle in DPS2 composite. From the figure, Si and C peaks can be observed from the elemental diffraction scanning analysis. Si, C peaks confirm the presence of SiC particles in the A357 matrix. Fig. 8(e) shows EDS analysis at the Al/SiC interface. The interface shows the presence of Mg peak along with Al, Si and C peaks. The presence of four elements Al, Mg, Si, and C confirms the presence of Mg_2Si at the Al-SiC interface.

3.5. *TEM analysis of A357 alloy and its DPS composite at T6-heat treated condition*

Precipitation is a very important aspect of age hardening which directly influences the mechanical properties of a material. Fig. 9 shows the bright-field TEM images of both A357 alloy and its composites with dual size SiC particles that were aged at 180 °C for about 6 h. TEM image of A357 alloy as depicted

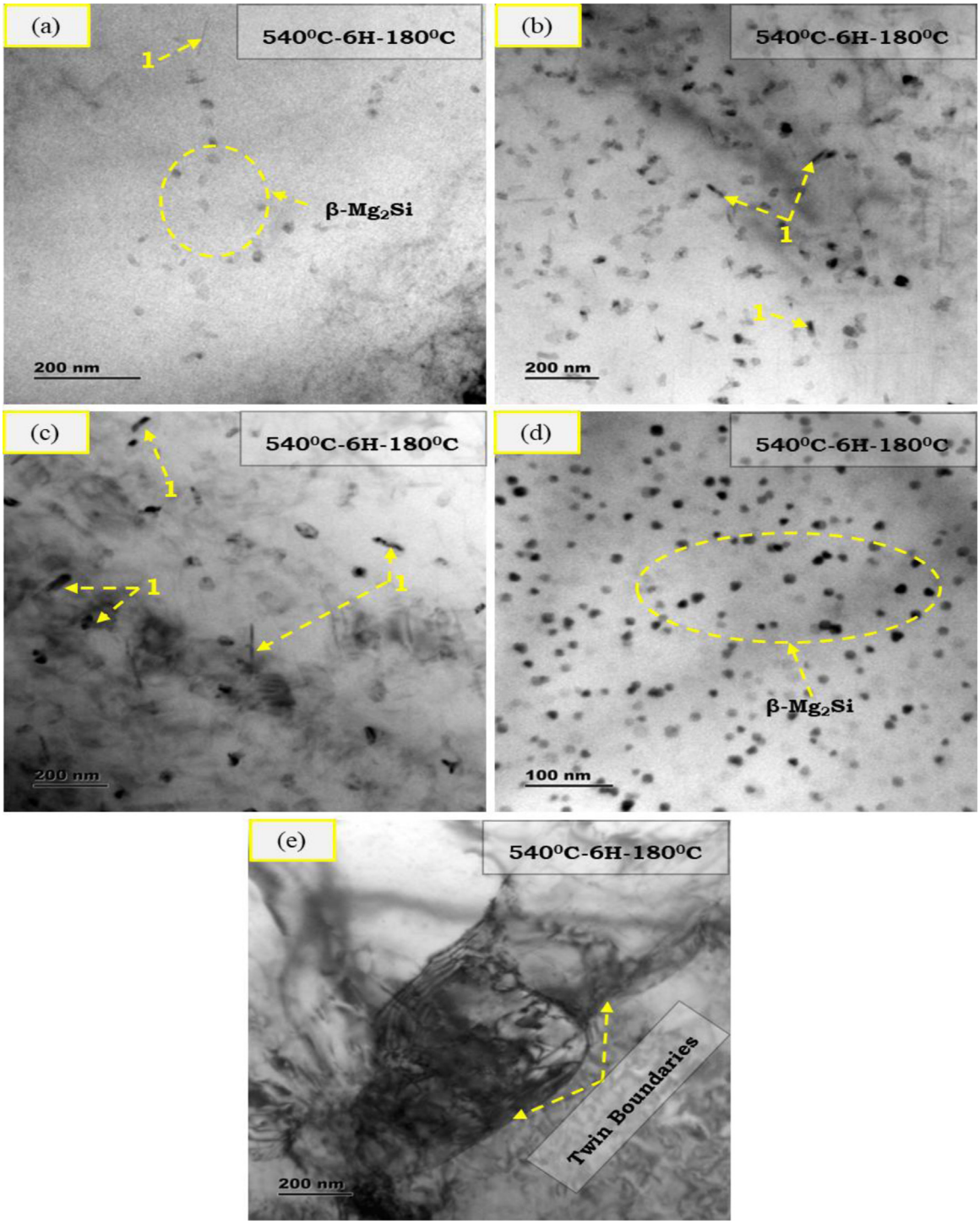

Fig. 9 – Bright-field TEM images of both A357 alloy and its DPS composites aged at 540 °C-6H-180 °C. (a) A357 alloy (b) DPS1 composite (c) DPS2 composite (d) DPS3 composite (e) modified Si particles with twins in DPS2 composite. From the Marking 1 represent needle shaped β″ phase.

in Fig. 9(a) shows the presence of very fine sized precipitates consisting of Mg and Si atoms. These fine shaped precipitates which were spherical in shape correspond to β–Mg_2Si with diameter in the range of 20–40 nm. Apart from these precipitates, few needles corresponding to β″ phase were also observed in the A357 alloy. In case of DPS1 and DPS2, along with the β–Mg_2Si precipitates, needles of β″ phase was also observed as shown in Fig. 9(b) and (c). Compared to A357 alloy, needle shaped β″ phase was comparatively high in case of these composites. Most of these fine needles had length in the range of 30–100 nm and diameter of about ~5 nm in the peak-aged heat-treated conditions. Due to high silicon content in

the matrix, quenching gives rise to higher content of supersaturated Si which favors the formation of β″ phase [49]. Further a high magnification TEM micrograph as shown in Fig. 9(d) of DPS3 composite showed uniform dispersion of β–Mg_2Si precipitates in the entire α-Al matrix. Further, presence of high silicon content in A357 matrix required above the stoichiometric formation of β–Mg_2Si will not only favor the nucleation of these precipitates but also strength of both A357 alloy and DPS composites. However, it is interesting to note that in both A357 alloy and composites, no β′ phase was observed which otherwise is considered to be nucleation site for β″ phase [50,51]. Fig. 9(e) shows a small crystal of silicon particle whose edges are more rounded indicating spheroidization. Dark contrast structures resembling twin boundaries and dislocation networks are also seen inside the silicon particle. The morphological changes from irregular to nearly round shape and decrease in size from coarse to small are mainly due to solution treatment. In addition to this, formation of β′ precipitates generate stresses in the matrix which is compensated by the modification in silicon particle [52].

3.6. *Influence of aging temperature on tensile properties of A357 alloy and its DPS composites*

Fig. 10(a) and (b) show the variation of tensile strength (ultimate & yield) of A357 alloy and its DPS composites at varying aging temperatures (160 °C, 180 °C, and 200 °C). From Fig. 10(a) and (b) it can be observed that the addition of particulate reinforcement enhances the tensile strength of the composites [53,54]. Although all composites subjected to heat treatment give nearly same tensile strength (ultimate & yield) values, the DPS3 composite exhibited slightly better strength properties in all three aging conditions followed by DPS1 and DPS2. Strengthening effect in composites can be attributed to number of particles present in a composite. Even though, the weight fraction of SiC is same for all composites, number of particles is highest in DPS3 because of large fraction of small particles. After DPS3, DPS1 and DPS2 have more number of smaller particles in that order. SiC particles act as dislocation pinning sites and hence can improve strength. Possible grain refinement due to SiC particles and effective load transfer

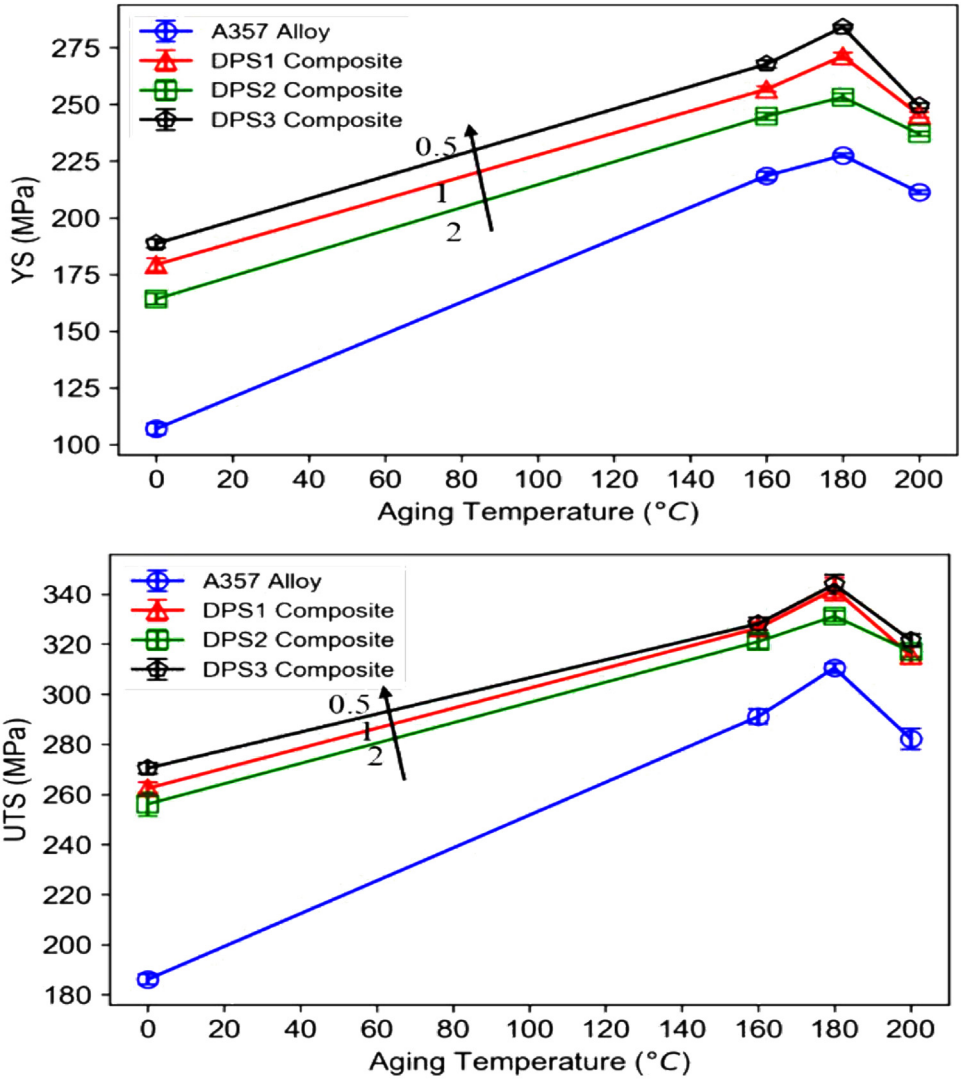

Fig. 10 – Tensile test results of A357 alloy and its DPS composites at varying aging temperatures. Arrows indicate direction of increasing strength and numbers on lines indicate ratio of large to small particles.

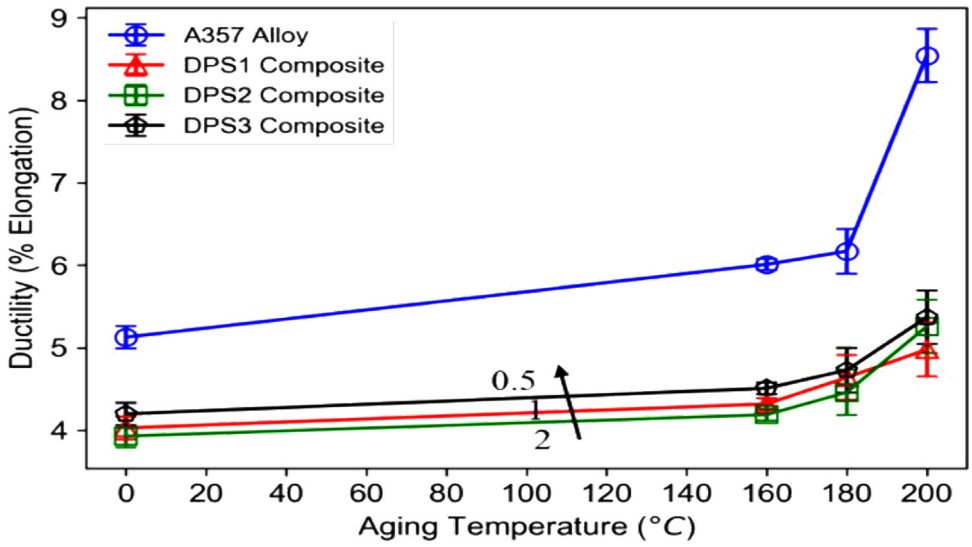

Fig. 11 – Ductility results of A357 alloy and its DPS composites at varying aging temperatures. Arrow indicates direction of increasing ductility and numbers on lines indicate ratio of large to small particles.

from matrix to composite particles are also expected to play a role in increase in the strength values of composites. So, the strengthening of composites is a result of synergistic effect of grain refinement, precipitation hardening, Orowan looping and efficient load transfer [55–60].

Further, from Fig. 10(a) and (b), it can be observed that the strength values increase with increase in aging temperature from 160 °C to 180 °C but tend to drop as the temperature is increased to 200 °C. It should be noted that highest strength values are observed at 180 °C aging temperature. Upon aging, increase in strength properties are due to precipitation of coherent β–Mg_2Si particles. Upon over aging, loss in coherence leads to loss in strength.

Fig. 11 shows the variation of percentage elongation of A357 alloy and its DPS composites at varying aging temperatures. From Fig. 11, it can be seen that the composites exhibit lower ductility (measured as % elongation) when compared to the alloy at all aging temperatures. Presence of SiC particles could lead to reduction in ductility because they can act as nucleation sites for cracks and thus hasten failure. The mechanism of fracture appears to be changing from alloy to composites. Also, from Fig. 11, it can be observed that as the aging temperature increases ductility increases substantially for A357 alloy whereas it increases marginally for composites. Increase in ductility in A357 alloy with aging temperature could be due to change in fracture mechanism from interdendritic to intra dendritic upon over aging (Fig. 12(a) and (b)). Whereas for composites, aging temperature has little effect because fracture mechanism remains to be particle pull out irrespective of aging temperature (Fig. 12(c)–(h)). Analogous trends have been reported in literature [52].

3.7. *Fractographs of A357 alloy and its DPS composites at varying aging temperatures*

Tensile fracture surfaces of A357 alloy and its DPS composites were analyzed using SEM and are shown in Fig. 12(a)–(h). For the cases of 180 °C and 200 °C, large numbers of dendrite fractured regions were observed in the fractograph (Fig. 12(a) and (b)). This confirms inter-dendritic cracking as the main fracture mechanism as these dendrite globules promote micro-crack propagation during the loading [61]. On the other hand, all DPS composites (DPS1, DPS2 and DPS3) at both aging temperatures i.e. 180 °C for 6 h. and 200 °C for 6 h, showed nearly identical fracture surfaces. The fracture surfaces consisted of a large number of dimples indicating ductile failure by void nucleation and coalescence mechanisms. The void nucleation takes place at Al matrix/SiC interface. When stress is applied, the plastic deformation starts by dislocation movement. These dislocations are blocked by the Al matrix/SiC interfaces resulting in dislocation accumulation. This builds up the stress around the interfaces resulting in much higher stress than the applied stress. When the stress is sufficient to crack the interface, the micro void preferably nucleates at the interface due to strong stress gradient. Due to the creation of micro-voids, the crack initiates at the micro void and propagates around the SiC particles. Eventually, the particles are pulled out of the A357 matrix leaving behind nearly circular shaped voids. These voids connect with each other through crack propagation and finally lead to fracture forming a dimpled fractured surface as seen in Fig. 12(c)–(h).

3.8. *Influence of aging temperature on hardness of A357 alloy and its DPS composites*

Fig. 13 shows the variation of hardness of A357 alloy and its DPS composites at varying aging temperatures (160 °C, 180 °C, and 200 °C). The DPS composites showed an increase in hardness when compared to A357 alloy at varying aging temperatures. Higher hardness values of composites can be attributed to the presence of hard SiC particles. Among the composites, DPS2 composite shows highest hardness and DPS3 shows the lowest hardness at all three aging temperatures. This trend in hardness among composites can be

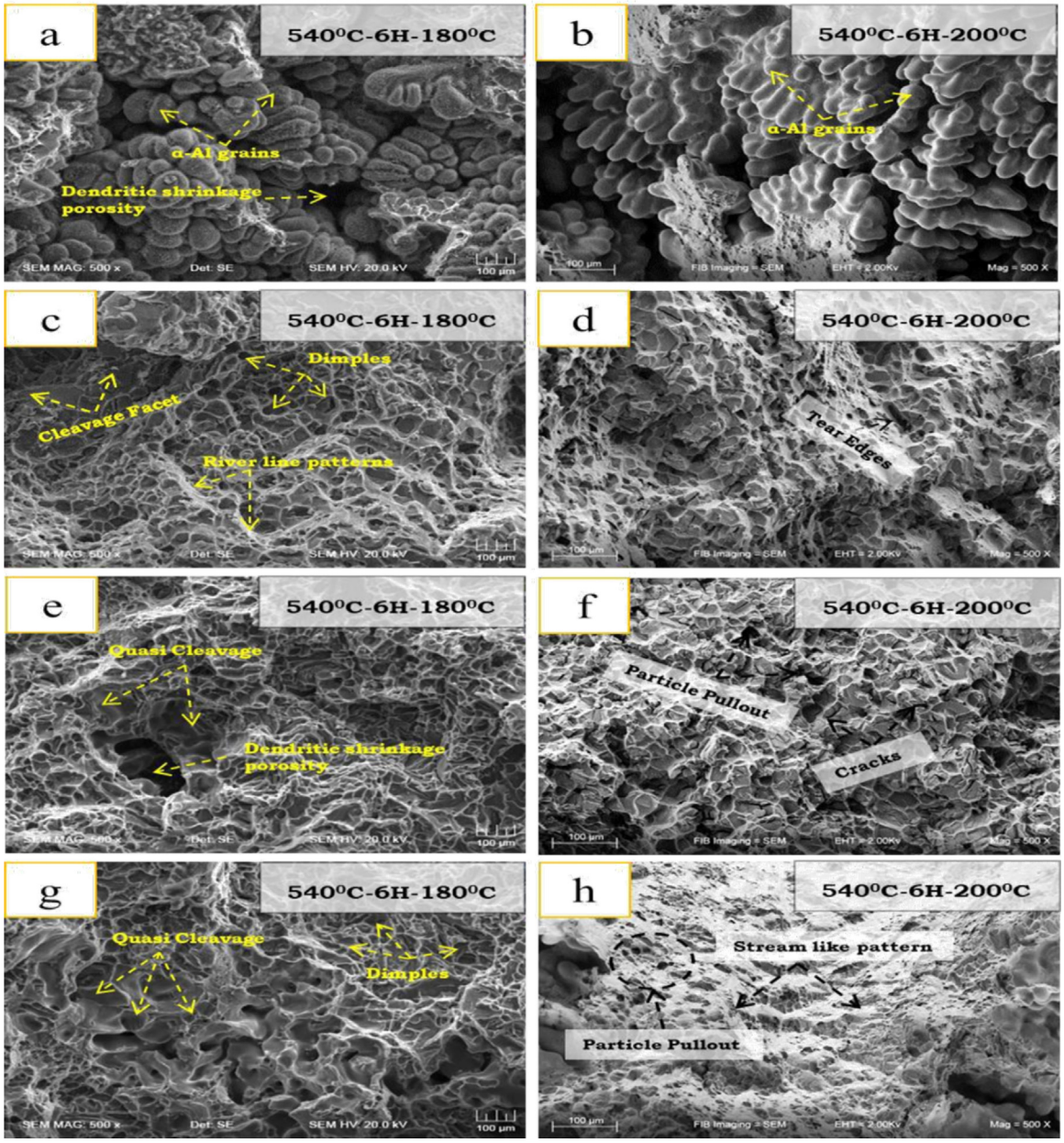

Fig. 12 – Fractographs of A357 alloy and its DPS Composites at varying aging temperatures. Where (a) & (b) A357 alloy at aging temperature of 180 °C and 200 °C, (c) & (d) DPS1 composite at aging temperature of 180 °C and 200 °C, (e) & (f) DPS2 composite at aging temperature of 180 °C and 200 °C, (g) & (h) DPS3 composite at aging temperature of 180 °C and 200 °C.

rationalized based on weight fraction of large SiC particles. Small size particles offer less resistance to deformation when compared to coarse size particles and hence leads to low hardness values [30,31]. Highest hardness of DPS2 composite is due to the presence of highest weight fraction of large sized particles. Similarly, lowest hardness values exhibited by DPS3 composite is due to the presence of lowest weight fraction of large sized particles.

From Fig. 13 it can be observed that the hardness values increase with aging temperature till 180 °C where it peaks and reduces beyond 180 °C. The increase in hardness after heat treatment can be attributed to formation of hard Mg_2Si phase due precipitation hardening [62]. According to the peak hardness variation with different aging temperatures, it was found that the composite is under aged at 160 °C and over-aged at 200 °C. Analogous trends were reported in literature [44,45,63].

3.9. *Specific wear rate of A357 alloy and its DPS composites at varying aging temperatures*

Fig. 14 shows the plot of specific wear rate (at 30 N) v/s aging temperature of A357 alloy and its DPS composites. From Fig. 14 it can be observed that as-cast alloy (A357) displayed the highest wear rate. The reason for highest wear rate in A357 alloy can be due to reasons such as extensive sub surface

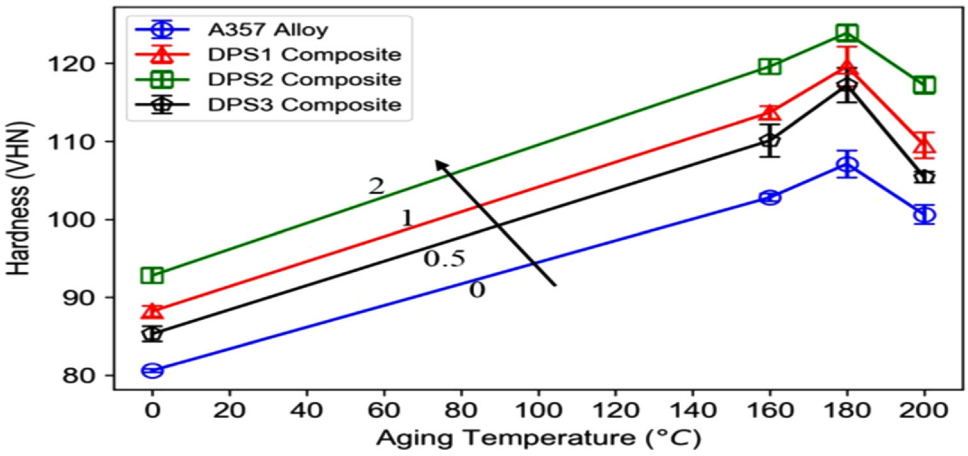

Fig. 13 – Hardness test results of A357 alloy and its DPS composites at varying aging temperatures. Arrow indicates direction of increasing hardness and numbers on lines indicate ratio of large to small particles.

deformation, high adhesive metal-metal contact assisted surface shear strain, the increased contact area of matrix to counter surface, and the absence of load bearing particles [30,31,64]. From Fig. 14, it can also be observed that DPS composites show less wear rate when compared to A357 alloy. This can be attributed to the presence of hard SiC particles in DPS composites. SiC particles are hard and hence they can resist abrasion. Moreover, they also reduce contact between counter surface and soft matrix and share some load. Reduced contact between counter surface and matrix and load sharing leads to reduced wear rate [65,66]. Among the composites, the DPS2 composite displayed least wear rate when compared to DPS1 and DPS3 composites at all aging temperatures. Good wear resistance (least wear rate) of DPS2 is mainly due to presence of high weight percent of large sized SiC particles which bear most of the applied pressure than that of small sized SiC particles and A357 matrix. Further, large sized SiC particle protect the small sized SiC particles from gouging out of the matrix thereby allowing them to provide protection against weight loss for a longer time [25,31,67–69]. It is interesting to note the relation between aging temperatures and wear resistance. From Fig. 14, it can be observed that both A357 alloy and its DPS composites show decrease in wear rate with aging temperature till 180 °C but beyond this temperature wear rate appears to be increasing. The specimens aged at 180 °C showed better wear resistance compared to the specimens aged at 160 °C and 200 °C and it may be due to the presence β″ and β-Mg_2Si precipitates [70,71]. Thus, the specimens aged at 180 °C can be considered as peak aged and the specimens which are aged at 160 °C are considered as under aged and the specimens which are aged at 200 °C are considered as over aged. Similar results were reported by several researchers [63,72].

3.10. *Worn surface analysis of A357 alloy and its DPS composites at varying aging temperature*

Worn surfaces of both A357 alloy and its DPS composites aged at different temperatures of 180 °C and 200 °C taken at 30 N load are shown in Fig. 15(a)–(h).

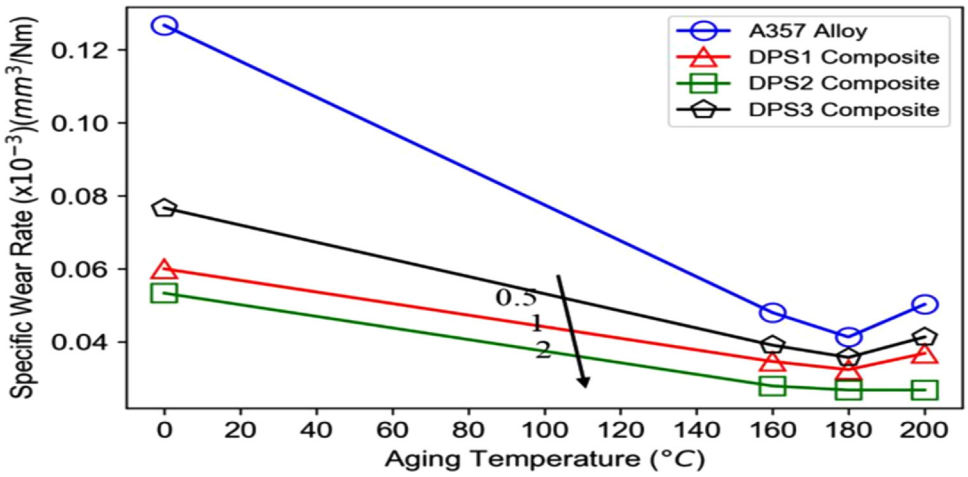

Fig. 14 – Effect of aging temperatures on wear rate of A357 alloy and its DPS composites. Arrow indicates the direction of lower specific wear rate and numbers on lines indicate ratio of large to small particles.

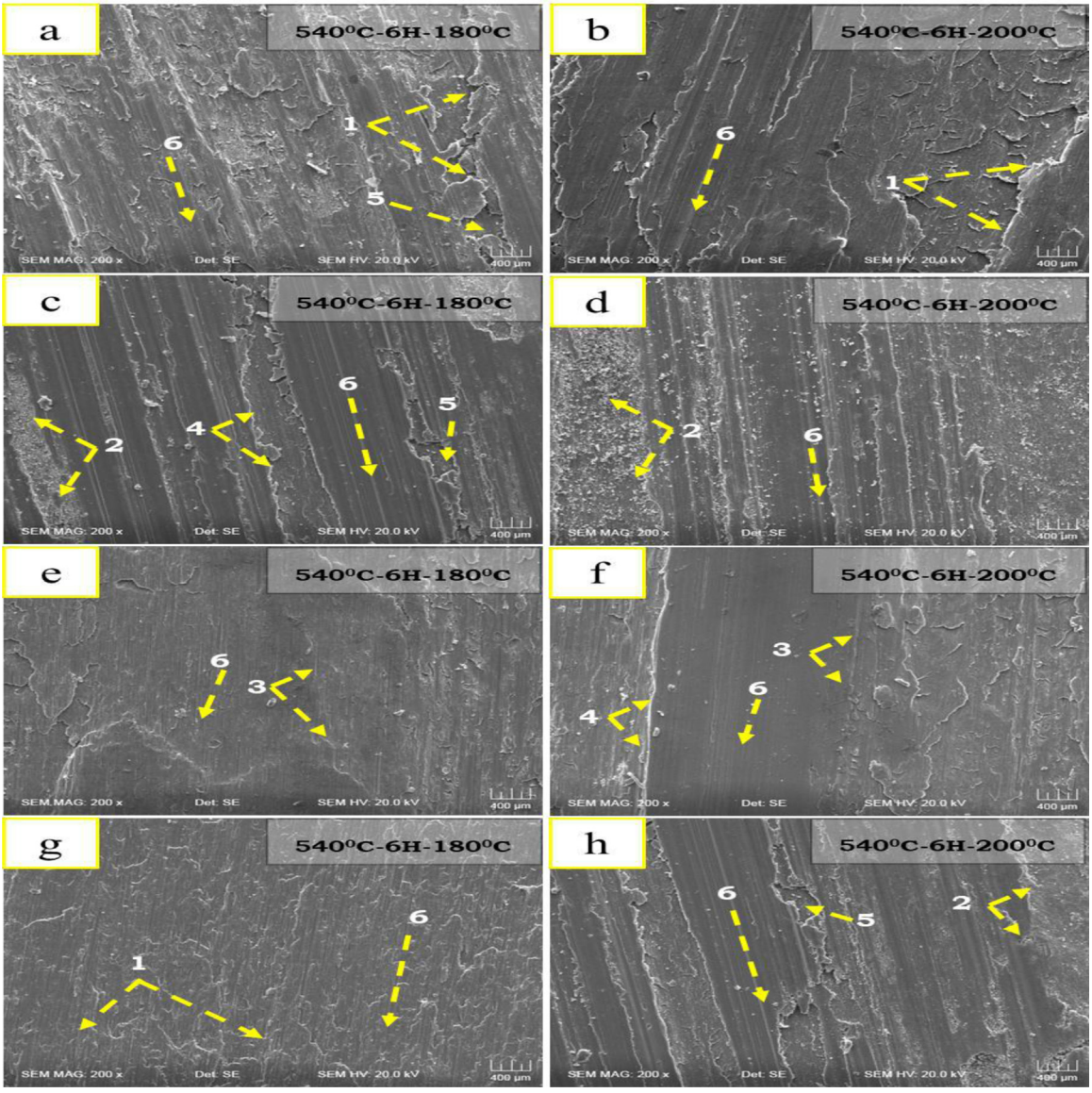

Fig. 15 – Wear tracks of A357 alloy and its DPS Composites at a load of 30 N, sliding velocity of 2.5 m/s and sliding distance of 1500 m subjected to varying Aging temperatures. Where (a) & (b) A357 alloy at aging temperatures of 180 °C and 200 °C, (c) & (d) DPS1 Composite at aging temperatures of 180 °C and 200 °C, (e) & (f) DPS2 composite at aging temperatures of 180 °C and 200 °C, (g) & (h) DPS3 Composite at aging temperatures of 180 °C and 200 °C. Markings 1–6 represent delaminated wear-out area, abrasion, thin ploughed trenches, deep ploughed trenches, craters, and sliding direction respectively.

Worn surface of A357 alloy at different aging temperatures (180 °C and 200 °C) is shown in Fig. 15(a) and (b). It is observed that wear mechanism changes with temperature. At peak aging temperature, 180 °C, wear is predominantly caused by the surface delamination. When temperature is increased to 200 °C, instead of surface delamination, deep grooves are observed which is an indication of plastic deformation. So, at high temperatures, wear mechanism changes from surface delamination to intense plastic deformation and material removal. Both the worn surfaces show wide and parallel grooves running in sliding direction with large cavities in between them. The formation of cavities can be attributed to delamination of surface material of the alloy. At a high load of 30 N, the softening of surface takes place due to frictional resistance as a result of surface material of the alloy getting welded to the counterface surface. Due to increase in adhesive nature of pin and alloy, delamination occurs easily. It appears that the extent of delamination is higher in case of 200 °C aged alloy which may be due to its low hardness when compared to that of 180 °C aging condition.

The extent of delamination appears to be less in DPS1 composite compared to that of the alloy as seen in Fig. 15(c) and (d). Hard SiC particles in DPS1 composite protrude out of composite surface during wear testing process and avoid direct contact between composite surface and counterface surface. Due to this, the extent of delamination is decreased.

The worn surface of DPS2 composite is nearly smooth for both aging temperatures as shown in Fig. 15(e) and (f). This is mainly due to presence of higher weight fraction of large size SiC particles which tend to take most of the applied load and protect small sized SiC particles as well as the matrix [73,74]. These large particles avoid direct contact between the counter-face surface and composite surface which is why the groove width is smaller when compared to that of A357 alloy and other two composites.

On the other hand, the worn surface of DPS3 composite was almost similar to that of DPS1 composite. Deformation grooves and delamination were the primary reasons of weight loss in this composite. The worn surface of DPS3 composite at two aging temperatures of 180 °C and 200 °C as shown in Fig. 15(g) and (h) show changes in the deformation mechanism from delamination at 180 °C aging temperature to deformation at 200 °C aging temperature.

3.11. *Three-dimensional surface topographies of worn surface A357 alloy and its DPS composites at varying aging temperatures*

Three-dimensional surface topographies of the worn surface of A357 alloy and its DPS composites taken at a load of 30 N, sliding velocity of 2.5 m/s and sliding distance of 1500 m are shown in Fig. 16(a)–(h). In case of A357 alloy, it can be seen from Fig. 16(a) and (b) that the surface showed features of surface delamination and formation of deep grooves supporting the evidence obtained using SEM (as shown in Fig. 15(a) and (b)). Further compared to a Ra value of 8.00 μm at 180 °C aging temperature the alloy aged at 200 °C showed higher Ra value of 8.44 μm. Lowest Ra values of 2.60 and 2.71 μm were obtained at aging temperature of 180 and 200 °C for DPS2 composite. These observations are well in line with the low specific wear rate obtained for this composite. Further, compared to A357

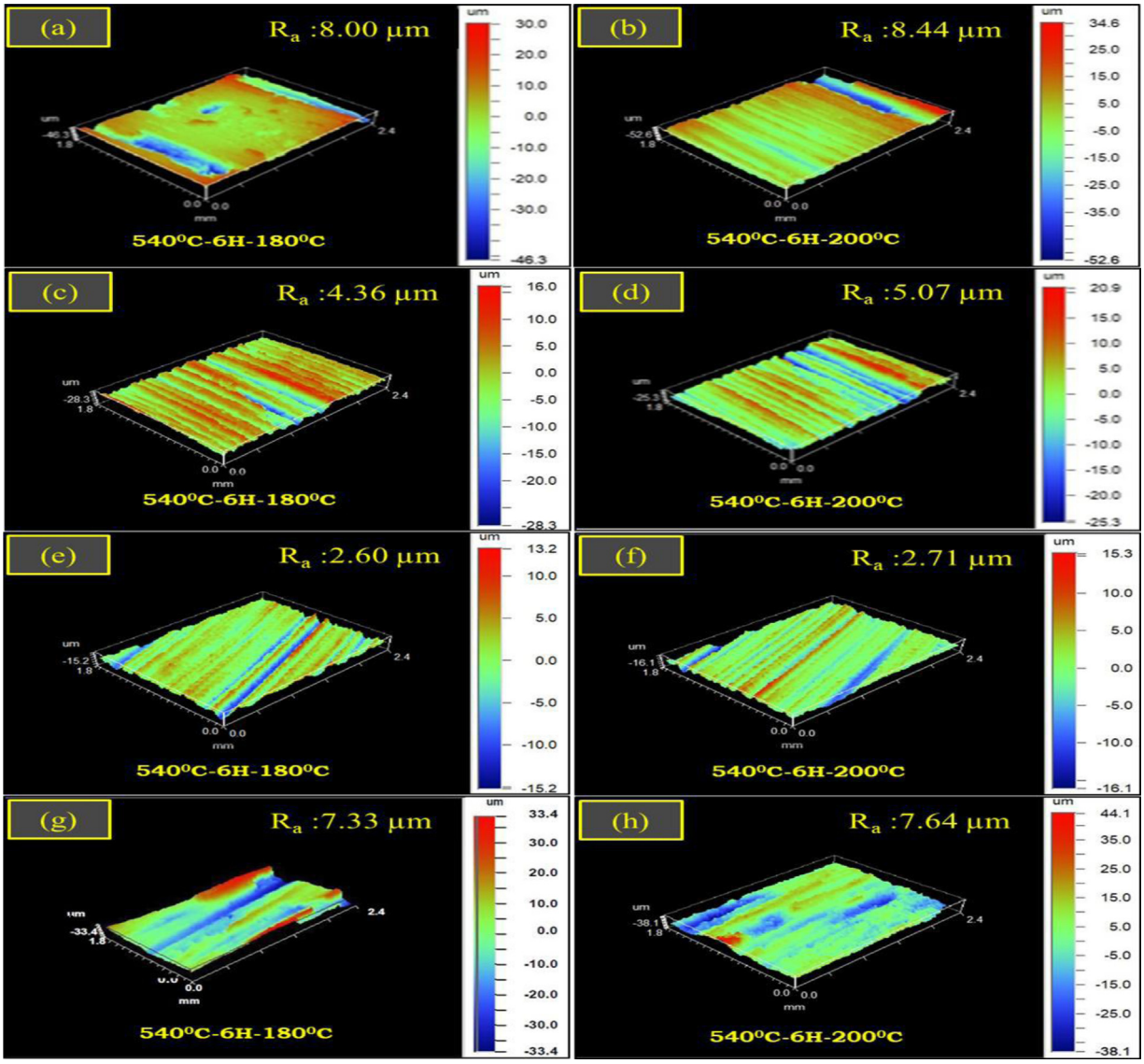

Fig. 16 – Three-dimensional surface topographies of the worn surface of A357 alloy and its DPS composites at a load of 30 N, sliding velocity of 2.5 m/s and sliding distance of 1500 m subjected to varying aging temperatures. Where (a) & (b) A357 alloy at aging temperatures of 180 °C and 200 °C, (c) & (d) DPS1 composite at aging temperatures of 180 °C and 200 °C, (e) & (f) DPS2 composite at aging temperatures of 180 °C and 200 °C, (g) & (h) DPS3 composite at aging temperatures of 180 °C and 200 °C.

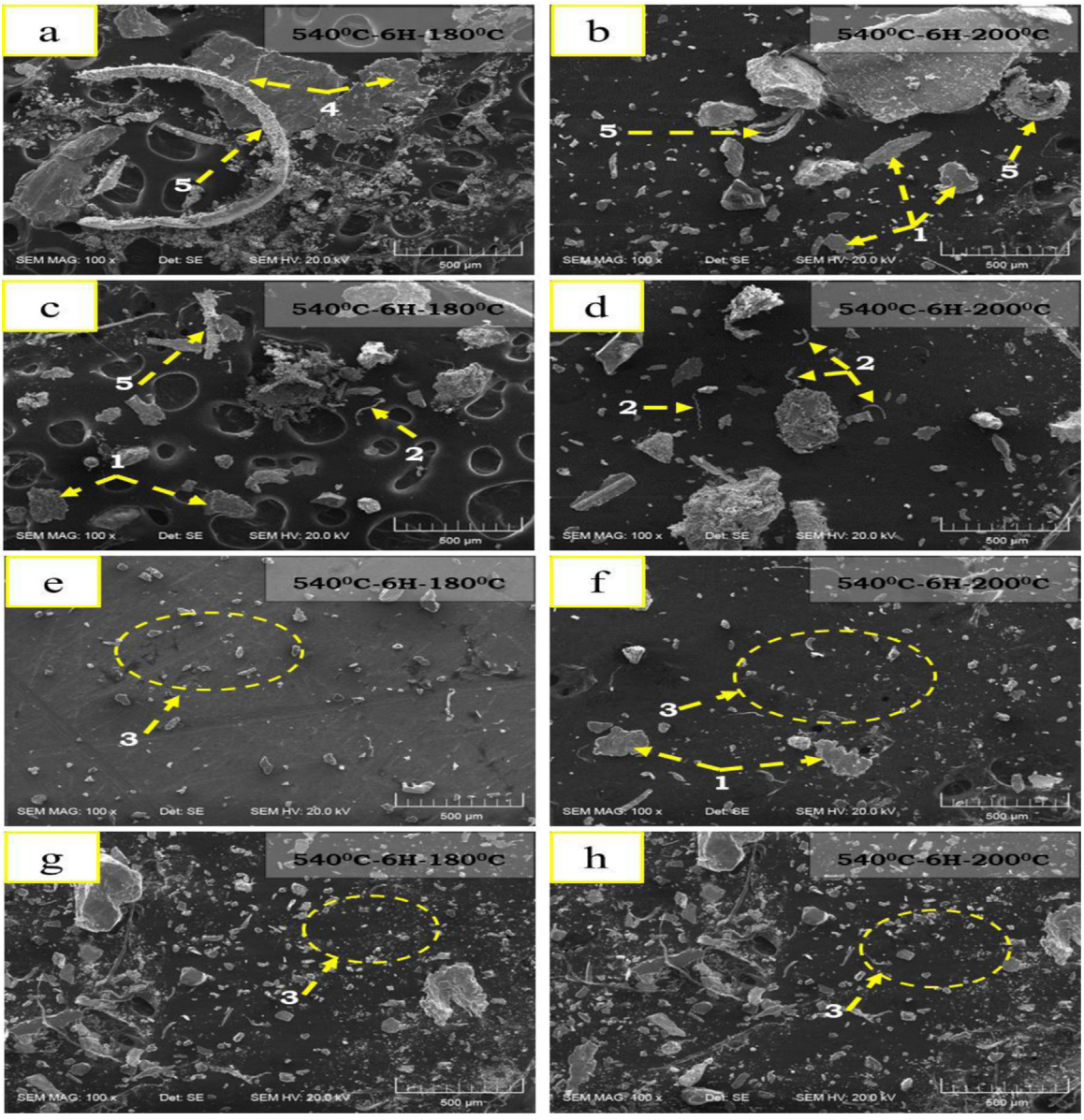

Fig. 17 – Wear debris of A357 alloy and its DPS Composites at a load of 30 N, sliding velocity of 2.5 m/s and sliding distance of 1500 m subjected to varying aging temperatures. Where (a) & (b) A357 alloy at aging temperatures of 180 °C and 200 °C, (c) & (d) DPS1 composite at aging temperatures of 180 °C and 200 °C, (e) & (f) DPS2 composite at aging temperatures of 180 °C and 200 °C, (g) & (h) DPS3 composite at aging temperatures of 180 °C and 200 °C. Markings 1–5 represent fleck-like debris, fiber-like debris, ruptured debris, ribbed debris and coil like debris respectively.

alloy and other composites the undulations observed on worn surface of DPS 2 is significantly less (see Fig. 15(e) and (f)). Also, compared to A357 alloy, the DPS composites showed lesser Ra values which is attributed to resistance offered by dual size SiC particles. The asperities of counterface surface are prevented from penetrating inside the matrix by the SiC particles due to which the surface roughness values are quite lesser for DPS composites. Unlike in several works [75,76] where the composites showed greater undulations as compared to alloy, here in this work no such observations were made. The depth of valleys and width of grooves were found to be higher for A357 alloy compared to that of DPS composites. This is mainly because of higher hardness values for DPS composites as compared to A357 alloy. Overall these results are well in line with preceding sub-sections (3.9 and 3.10). Further, compared to DPS composites A357 alloy exhibited higher Ra values due to higher wear rate. Along with this the surface topographies of DPS composites showed no abnormal depth in the worn surface indicating absence of pull-out of SiC particles.

3.12. *Wear debris analysis of A357 alloy and its DPS composites at varying aging temperature*

Wear debris was collected from both A357 alloy and its DPS composites after 180 °C and 200 °C aging temperatures for a fixed load of 30 N, sliding velocity of 2.5 m/s and sliding

distance of 1500 m. In the case of A357 alloy the size of wear debris collected for 180 °C was much smaller (~300 μm) than that collected for 200 °C (~600 μm) which is shown in Fig. 17(a) and (b). In the case of DPS1 composite the size of wear debris showed similar trend as that of A357 alloy. Wear debris size of ~100 μm and ~180 μm was obtained for the composite aged at 180 °C and 200 °C respectively as shown in Fig. 17(c) and (d). On the other hand, DPS2 composite wear debris as shown in Fig. 17(e) and (f) have sizes approximately ~50 μm and 100 μm for the composites aged at 180 °C and 200 °C respectively. The wear debris size of DPS2 composite is very small when compared to that of A357 alloy and other two composites. Most of the debris had irregular flake like morphology with sharp edges indicating delamination as primary wear mechanism. The small size of wear debris can be attributed to highest hardness of DPS2 composite for all cases of aging temperature. Similarly, for DPS3 composite, wear debris has a size of 150 μm and 200 μm approximately for the samples aged at 180 °C and 200 °C respectively as shown in Fig. 17(g) and (h). The wear debris size and morphology of DPS3 composites is almost same for both the aging temperatures as shown in Fig. 17(g) and (h). Overall it can be observed that at peak aging temperature of 180 °C, both A357 alloy and DPS composites showed smaller wear debris size which is attributed to the presence of uniformly dispersed hardening phases such as β″ and β-Mg_2Si precipitates compared to the over aged condition.

3.13. *Effect of ratio of DPS particles on mechanical and wear properties of DPS composites*

It is well known that DPS composites show better mechanical and wear properties compared to single particle reinforced composites. DPS composites have both small size and large size particles in varying proportion. However, it is not clear what should be a good proportion of large and small sized particles that would give optimum mechanical and wear properties. This question has not been studied in earlier works. From this work, it was found that small sized particles are good for strength properties while large sized particles are good for hardness and wear properties.

From Fig. 10(a) and (b) we see that high YS and UTS are realized when small sized particle proportion is higher (at L:S = 0.5). Ductility also shows similar trend as that of strength (refer Fig. 11) and it is better when the composite has higher proportion of small particles (at L:S = 0.5). However, good hardness and wear properties are obtained when the proportion of large particles is higher (L:S = 2) as shown in Figs. 13 and 14. As explained in pervious sections, good hardness and wear properties are mainly due to large sized particles taking the load and hence composites with higher ratio of L:S are good for wear properties. Whereas, strength and ductility are mainly the result of dislocation pinning and bowing which are good when particle size is smaller. Hence smaller particles are good for strength properties.

4. Conclusions

The following conclusions were drawn from the present work:

1. Mechanical and wear properties of A357 composite reinforced with dual size SiC particles were studied after aging at varying temperatures ((540 °C-6H-160 °C, 540 °C-6H-180 °C and 540 °C-6H-200 °C)).
2. Microscopy analysis showed fairly uniform dispersion of dual size SiC particles in A357 matrix.
3. From the density measurements of A357 alloy and its DPS composites at varying temperatures it can be concluded that the dispersion of SiC particles was found to be good with almost no observable porosity or any casting defects.
4. TEM analysis showed the formation of β”-semi-coherent phase and Mg_2Si precipitate (β-phase) along with SiC particles. These phases lead to the improvement in mechanical & wear properties in both A357 alloy and its DPS composites.
5. All the composites (DPS1, DPS2 and DPS3) showed improvement in mechanical and wear properties when compared to A357 alloy.
6. Overall, it can be concluded that for the same total weight percentage of SiC reinforcement, ratio of large to small particles influences mechanical and wear properties. Higher proportion of smaller particles improve strength and ductility whereas, higher proportion of larger particles improve hardness and wear properties.

Conflicts of interest

The authors declare no conflicts of interest.

REFERENCES

[1] Kumar RV, Keshavamurthy R, Perugu CS, Koppad PG, Alipour M. Influence of hot rolling on microstructure and mechanical behaviour of Al6061-ZrB_2 in-situ metal matrix composites. Mater Sci Eng A 2018;738:344–52.
[2] Mirjavadi SS, et al. Effect of hot extrusion and T6 heat treatment on microstructure and mechanical properties of Al-10Zn-3.5 Mg-2.5 Cu nanocomposite reinforced with graphene nanoplatelets. J Manuf Process 2018;36:264–71.
[3] Sethuram D, Koppad PG, Shetty H, Alipour M, Kord S. Characterization of graphene reinforced Al-Sn nanocomposite produced by mechanical alloying and vacuum hot pressing. Mater Today Proc 2018;5(11):24505–14.
[4] Mirjavadi SS, et al. Effect of multi-pass friction stir processing on the microstructure, mechanical and wear properties of AA5083/ZrO_2 nanocomposites. J Alloys Compd 2017;726:1262–73.
[5] Ceschini L, Morri A, Morri A, Gamberini A, Messieri S. Correlation between ultimate tensile strength and solidification microstructure for the sand cast A357 aluminium alloy. Mater Des 2009;30(10):4525–31.
[6] Wang Q, Davidson C. Solidification and precipitation behaviour of Al-Si-Mg casting alloys. J Mater Sci 2001;36(3):739–50.
[7] Tan Y-H, Lee S-L, Lin Y-L. Effects of Be and Fe additions on the microstructure and mechanical properties of A357. 0 alloys. Metall Mater Trans A 1995;26(5):1195–205.
[8] Edwards G, Stiller K, Dunlop G, Couper M. The precipitation sequence in Al–Mg–Si alloys. Acta Mater 1998;46(11):3893–904.

[9] Wang Q. Microstructural effects on the tensile and fracture behavior of aluminum casting alloys A356/357. Metall Mater Trans A 2003;34(12):2887–99.
[10] Canakci A, Varol T, Nazik C. Effects of amount of methanol on characteristics of mechanically alloyed Al-Al_2O_3 composite powders. Mater Technol 2012;27:320–7.
[11] Canakci A, Varol T, Ertok S. The effect of mechanical alloying on Al_2O_3 distribution and properties of Al_2O_3 particle reinforced Al-MMCs. Sci Eng Compos 2012;19:227–35.
[12] Canakci A, Varol T. A novel method for the production of metal powders without conventional atomization process. J Clean Prod 2015;99:312–9.
[13] Canakci A, Arslan F, Varol T. Physical and mechanical properties of stir casting processed AA2024/B_4Cp composites. Sci Eng Compos Mater 2014;21:505–15.
[14] Canakci A, Arslan F, Varol T. Effect of volume fraction and size of B_4C particles on production and microstructure properties of B_4C reinforced aluminum alloy composites. Mater Sci Technol 2013;29:954–60.
[15] Canakci A, Ozsahin S, Varol T. Prediction of effect of reinforcement size and volume fraction on the abrasive wear behavior of AA2014/B_4Cp MMCs using artificial neural network. Arab J Sci Eng 2014;39:6351–61.
[16] Zulfia A, Atkinson HV, Jones H, King S. Effect of hot isostatic pressing on cast A357 aluminium alloy with and without SiC particle reinforcement. J Mater Sci 1999;34:4305–10.
[17] Badizi RM, Askari-Paykani M, Parizad A, Shahverdi HR. Effects of electromagnetic frequency and SiC nanoparticles on the microstructure refinement and mechanical properties of Al A357-1.5 wt% SiC nanocomposites. Int J Metal Cast 2018;12:565–73.
[18] Datta J, Datta S, Banerjee MK, Bandyopadhyay S. Effect of scandium addition on the corrosion behavior of Al–Si–Mg–SiC_p metal matrix composites. Composites: Part A 2004;35:1003–8.
[19] Yu B, Zhang YJ, Zhao Z, Zhao F, Cai Q, Liu C. The reinforcing mechanism of TiB_2 in TiB_2/A357 composite. Acta Metall Sin Engl Lett 2009;16(5):375–8.
[20] Kandemir S. Microstructure and mechanical properties of A357/SiC nanocomposites fabricated by ultrasonic cavitation-based dispersion of ball-milled nanoparticles. J Compos Mater 2017;51(3):395–404.
[21] Leonard A, Perrin C, Rainforth W. Microstructural changes induced by dry sliding wear of a A357/SiC metal matrix composite. Mater Sci Technol 1997;13(1):41–8.
[22] Bloyce A, Summers J. Static and dynamic properties of squeeze-cast A357-SiC particulate Duralcan metal matrix composite. Mater Sci Eng A 1991;135:231–6.
[23] Taghiabadi R, Mahmoudi M, Emamy Ghomy M, Campbell J. Effect of casting techniques on tensile properties of cast aluminium alloy (Al–Si–Mg) and TiB_2 containing metal matrix composite. Mater Sci Technol 2003;19(4):497–502.
[24] Zhang LJ, Qiu F, Wang J-G, Wang H-Y, Jiang Q-C. Microstructures and mechanical properties of the Al2014 composites reinforced with bimodal sized SiC particles. Mater Sci Eng A 2015;637:70–4.
[25] Bindumadhavan P, Wah HK, Prabhakar O. Dual particle size (DPS) composites: effect on wear and mechanical properties of particulate metal matrix composites. Wear 2001;248(1–2):112–20.
[26] Arora R, Kumar S, Singh G, Pandey O. Influence of particle size and temperature on the wear properties of rutile-reinforced aluminium metal matrix composite. J Compos Mater 2015;49(7):843–52.
[27] Zhang Q, Wu G, Sun D, Chen G, Jiang L. Microstructure and thermal conduction properties of an Al-12Si matrix composite reinforced with dual sized SiC particles. J Mater Sci 2004;39(1):303–5.
[28] Sharma S, Nanda T, Pandey O. Effect of dual particle size (DPS) on dry sliding wear behaviour of LM30/sillimanite composites. Tribol Int 2018;123:142–54.
[29] Yang MJ, Zhang DM, Gu XF, Zhang LM. Effects of SiC particle size on CTEs of/Al composites by pulsed electric current sintering. Mater Chem Phys 2006;99:170–3.
[30] Avinash L, Ramprabhu T, Bontha S. The Effect on the dry sliding wear behavior of gravity cast A357 reinforced with dual size silicon carbide particles. Appl Mech Mater 2016;829:83–9.
[31] Lakshmikanthan A, Bontha S, Krishna M, Koppad PG, Ramprabhu T. Microstructure, mechanical and wear properties of the A357 composites reinforced with dual sized SiC particles. J Alloys Compd 2019;786:570–80.
[32] Apelian D, Shivkumar S, Sigworth G. Fundamental aspects of heat treatment of cast Al-Si-Mg alloys. AFS Trans 1989;97:727–42.
[33] Shivkumar S, Keller C, Trazzera M, Apelian D. Precipitation hardening in A356 alloys. In: Production, refining, fabrication and recycling of light metals. Elsevier; 1990. p. 264–78.
[34] Handbook A. Heat treating. ASM Int 1991;4(10).
[35] Ajith Kumar KK, Viswanath A, Rajan TPD, Pillai UTS, Pai BC. Physical, mechanical, and tribological attributes of stir-cast AZ91/SiC_p composite. Acta Metall Sin (Engl Lett) 2014;27:295–305.
[36] Prasada DS, Shobab C, Ramanaiah N. Investigations on mechanical properties of aluminum hybrid composites. J Mater Res Technol 2014;3(1):79–85.
[37] Hu Y, Wu T, Guo Y, Wang W, Song M, Qian L, et al. Effects of T6 treatment, tensile temperature, and mass fraction of SiC on the mechanical properties of SiCp/6061Al composites. Materials 2019;12:1602.
[38] Rao C, Selvaraj N, Veereshkumar G. Studies on mechanical and dry sliding wear of Al6061–SiC composites. Compos B Eng 2012;43(3):1185–91.
[39] T. Ram Prabhu, M. Murugan, B.P. Chiranth, R.K. Mishra,N. Rajini,P. Marimuthu, P. Dinesh Babu, G. Suganya Effects of Dual-Phase Reinforcement Particles (Fly Ash + Al_2O_3)on the Wear and Tensile Properties of the AA 7075 Al Alloy Based Composites.
[40] Aversa A, Lorusso M, Trevisan F, Ambrosio EP, Calignano F, Manfredi D, et al. Effect of process and post-process conditions on the mechanical properties of an A357 alloy produced via laser powder bed fusion. Metals 2017;7(2):68.
[41] Akhter R, Ivanchev L, Burger H. Effect of pre/post T6 heat treatment on the mechanical properties of laser welded SSM cast A356 aluminium alloy. Mater Sci Eng A 2007;447(1–2):192–6.
[42] Maube SE, Wangombe DN, Maranga SM, Kihiu JM. Effect of cooling rate and heat treatment on the microstructure and impact resistance of recycled aluminium sand cast alloy. J Sustain Res Eng 2014;1(1).
[43] Cottu JP, Couderc JJ, Viguier B, Bernard L. Influence of SiC reinforcement on precipitation and hardening of a metal matrix composite. J Mater Sci 1992;27:3068–74.
[44] Yamanoğlu R, Karakulak E, Zeren A, Zeren M. Effect of heat treatment on the tribological properties of Al–Cu–Mg/nanoSiC composites. Mater Des 2013;49:820–5.
[45] Myriounis D, Hasan S, Matikas T. Heat treatment and interface effects on the mechanical behavior of SiC-particle reinforced aluminium matrix composites. J ASTM Int 2008;5(7):1–10.
[46] Christman T, Suresh S. Microstructural development in an aluminum alloy-SiC whisker composite. Acta Metall 1988;36(7):1691–704.
[47] Manoharan M, Lewandowski J. In-situ deformation studies of an aluminum metal-matrix composite in a scanning electron microscope. Scr Metall 1989;23(10):1801–4.

[48] Karuppusamy T, Velmurugan C, Thirumalaimuthukumaran M. Experimental study on the mechanical properties of heat treated aluminium composites. Mater Res Express 2019;6:096552.
[49] Sjolander E, Seifeddine S. The heat treatment of Al–Si–Cu–Mg casting alloys. J Mater Process Technol 2010;210(10):1249–59.
[50] Li B, Luo B, He K, Zeng L, Fan W, Bai Z. Effect of aging on interface characteristics of Al–Mg–Si/SiC composites. J Alloys Compd 2015;649:495–9.
[51] Liu C, Ma P, Zhan L, Huang M, Li J. Solute Sn-induced formation of composite β′/β precipitates in Al-Mg-Si alloy. Scr Mater 2018;155:68–72.
[52] Wang T, Zhao Y, Chen Z, Zheng Y, Kang H. The bimodal effect of La on the microstructures and mechanical properties of in-situ A356–TiB_2 composites. Mater Des 2015;85:724–32.
[53] Arsenault R, Everett R. Tensile and compressive properties of metal matrix composites 4. Academic Press; 1991.
[54] Ganesh V, Chawla N. Effect of particle orientation anisotropy on the tensile behavior of metal matrix composites: experiments and microstructure-based simulation. Mater Sci Eng A 2005;391(1–2):342–53.
[55] Mirjavadi SS, et al. Influence of TiO_2 nanoparticles incorporation to friction stir welded 5083 aluminum alloy on the microstructure, mechanical properties and wear resistance. J Alloys Compd 2017;712:795–803.
[56] Cai C, Geng H, Wang S, Gong B, Zhang Z. Microstructure evolution of AlSi10Mg (Cu) alloy related to isothermal exposure. Materials 2018;11(5):809.
[57] Bembalge O, Panigrahi S. Development and strengthening mechanisms of bulk ultrafine grained AA6063/SiC composite sheets with varying reinforcement size ranging from nano to micro domain. J Alloys Compd 2018;766:355–72.
[58] Umaru O, Abdulwahab M, Tokan A, Bello A, Umar H. Effect of double thermal ageing treatment on the mechanical properties of Al–Cu–Mg/3% rice husk ash composite. Results Phys 2016;6:342–5.
[59] Zhu H, Guo J, Jia J. Correlation of the aging characteristics and deformation behavior of A357 alloy. J Mater Eng Perform 2001;10(2):186–91.
[60] Prabhu TR. Effects of ageing time on the mechanical and conductivity properties for various round bar diameters of AA 2219 Al alloy. Eng Sci Technol Int J 2017;20(1):133–42.
[61] Chen Z, Hao X, Wang Y, Zhao K. In-situ observation of tensile fracture in A357 casting alloys. J Mater Sci Technol 2014;30:139–45.
[62] Sharma V, Kumar S, Panwar RS, Pandey O. Microstructural and wear behavior of dual reinforced particle (DRP) aluminum alloy composite. J Mater Sci 2012;47(18):6633–46.
[63] Ravikumar M, Reddappa H, Suresh R. Study on mechanical and tribological characterization of Al_2O_3/SiCp reinforced aluminum metal matrix composite. Silicon 2018;10(6):2535–45.
[64] Prabhu TR. Effect of bimodal size particles reinforcement on the wear, friction and mechanical properties of brake composites. Tribol – Mater Surf Interfaces 2016;10(4):163–71.
[65] Rao R, Das S, Mondal D, Dixit G. Dry sliding wear behaviour of cast high strength aluminium alloy (Al–Zn–Mg) and hard particle composites. Wear 2009;267(9–10):1688–95.
[66] Rajeev V, Dwivedi D, Jain S. Effect of load and reciprocating velocity on the transition from mild to severe wear behavior of Al–Si–SiCp composites in reciprocating conditions. Mater Des 2010;31(10):4951–9.
[67] Chung S, Hwang BH. A microstructural study of the wear behaviour of SiCp/Al composites. Tribol Int 1994;27(5):307–14.
[68] Chawla KK. Metal matrix composites. Mater Sci Technol 2006.
[69] Song W, Krauklis P, Mouritz A, Bandyopadhyay S. The effect of thermal ageing on the abrasive wear behaviour of age-hardening 2014 Al/SiC and 6061 Al/SiC composites. Wear 1995;185(1–2):125–30.
[70] Pedersen L, Arnberg L. The effect of solution heat treatment and quenching rates on mechanical properties and microstructures in AlSiMg foundry alloys. Metall Mater Trans A 2001;32(3):525–32.
[71] Guan LY, Li BL, Qi P, Wei LJ, Nie ZR. Effect of heat treatment on the microstructure and property of Al-Si-Mg alloy. Mater Sci Forum 2016;850:768–72.
[72] Chacko M, Nayak J. Aging behaviour of 6061 Al-15 Vol% SiC composite in T4 and T6 treatments. Int J Chem Mol Nucl Mater Metall Eng 2014;8(3):195–8.
[73] Rajmohan T, Palanikumar K, Ranganathan S. Evaluation of mechanical and wear properties of hybrid aluminium matrix composites. Trans Nonferrous Met Soc China 2013;23(9):2509–17.
[74] Singh J, Chauhan A. Overview of wear performance of aluminium matrix composites reinforced with ceramic materials under the influence of controllable variables. Ceram Int 2016;42(1):56–81.
[75] Sardar S, Karmakar SK, Das D. Tribological properties of Al 7075 alloy and 7075/Al_2O_3 composite under two-body abrasion: a statistical approach. J Tribol 2018;140:051602.
[76] Sardar S, Pradhan SK, Karmakar SK, Das D. Modeling of abraded surface roughness and wear resistance of aluminum matrix composites. J Tribol 2019;141:0716.